

Supporting Information

Insights into Energy Transfer Pathways between Exciplex Host and Fluorescent Guest: Attaining Highly Efficient 710 nm Electroluminescence.

Chun-Ying Huang,^{1,†} Ssu-Yu Ho,^{1,†} Chien-Hsun Lai,² Chang-Lun Ko,² Yu-Chen Wei,¹ Jia-An Lin,¹ Deng-Gao Chen,¹ Tzu-Yu Ko,¹ Ken-Tsung Wong,¹ Zhiyun Zhang,^{3,*} Wen-Yi Hung,^{2,4*} and Pi-Tai Chou^{1,*}

¹ Department of Chemistry, National Taiwan University, Taipei 10617, Taiwan

² Department of Optoelectronics and Materials Technology, National Taiwan Ocean University, Keelung 202, Taiwan

³ Key Laboratory for Advanced Materials and Institute of Fine Chemicals, East China University of Science & Technology, Shanghai 200237, P.R. China.

⁴ Center of Excellence for Ocean Engineering, National Taiwan Ocean University, Keelung, 202, Taiwan

Prof. Pi-Tai Chou, E-mail: chop@ntu.edu.tw

Prof. Wen-Yi Hung, E-mail: wenhung@mail.ntou.edu.tw

Prof. Zhiyun Zhang, E-mail: zhangzhiyun@ecust.edu.cn

Table of Contents

Title	page
Experimental Section	S3
Simulative Approach	S7
Figure S1-2. The fluorescence decay dynamics of NOz-TPA and NOz-t-TPA in (a) CHX, (b) TOL, (c) DCM, and (d) neat thin film at RT. IRF denotes instrument response function.	S9-10
Figure S3. Population lifetime of Tris-PCz:CN-T2T:dopant ((a,b) for NOz-TPA and (c,d) for NOz-t-TPA) under 5 and 10%.	S11
Figure S4-5. Dynamic information of Tris-PCz:CN-T2T exciplex.	S12
Figure S6. Experimental HOMO value of the neat film of (a) NOz-TPA and (b) NOz-t-TPA .	S13
Figure S7. Cyclic voltammograms of NOz.	S13
Figure S8-9. Detailed device performance for NOz-TPA (S8), and NOz-t-TPA (S9) with different doping concentration.	S14-15
Figure S10-14. NMR spectra of the selected molecules.	S16-18
Table S1. Selected photophysical properties of NOz-TPA and NOz-t-TPA measured at RT.	S19
Table S2. Optimized structure of NOz-TPA and NOz-t-TPA in ground states (S_0) and the corresponding frontier orbitals.	S19
Table S3. Model Fitting Parameters.	S20
Table S4. The orbital energy levels for NOz-TPA and NOz-t-TPA .	S20

Experimental Section:

General Information. All reactions were performed under an atmosphere of nitrogen. If not specifically mentioned, solvents were used without drying. Commercially available reagents were used without purification. ^1H and ^{13}C NMR spectra were measured with a Varian Mercury-400 instrument at 400 and 100 MHz. The chemical shifts (δ) and the coupling constants (J) were recorded in parts per million (ppm), and in Hertz (Hz), respectively

Synthetic Procedures.

4,4'-(napho[1,2-c:5,6-c']bis([1,2,5]oxadiazole)-5,10-diyl)bis(N,N-diphenylaniline) (NOz-TPA). DiBr-NOz (0.30 g, 0.81 mmol) was dissolved in 1,4-dioxane (40 mL) under nitrogen atmosphere, followed by adding $\text{K}_2\text{CO}_{3(\text{aq})}$ (0.28 g, 2.0 mmol), (4-(diphenylamino)phenyl) boronic acid (0.94 g, 0.33 mmol) which is dissolved in ethanol and $\text{Pd}(\text{PPh}_3)_4$ (0.020 g, 0.017 mmol). The reaction mixture was stirred at reflux overnight and then cooled to room temperature. The solvent was concentrated under reduced pressure to give a crude product. The residue was washed by water and ethanol to give the purple powder **NOz-TPA** with a yield of 78% (0.44 g). ^1H NMR (400 MHz, CDCl_3) δ 8.55 (s, 2H), 8.05 (d, $J = 8.8$ Hz, 4H), 7.31 (t, $J = 7.6$ Hz, 8H), 7.21-7.18 (m, 12H), 7.10 (t, $J = 7.6$ Hz, 4H). ^{13}C NMR (100 MHz, CDCl_3) δ 149.54, 148.83, 148.47, 146.95, 129.52, 129.40, 127.20, 125.58, 125.42, 124.04, 122.99, 122.03, 121.53. HRMS (m/z , ESI, $[\text{M}+\text{H}]^+$) calcd. for $\text{C}_{46}\text{H}_{31}\text{N}_6\text{O}_2$ 699.2508, found 699.2507.

4-bromo-N,N-bis(4-(tert-butyl)phenyl)aniline (2). At room temperature, sodium *tert*-butoxide (0.47 g, 4.89 mmol) was added to a stirred solution of 1,1'-bis(diphenylphosphine)ferrocene (0.046 g, 0.083 mmol) and tris(dibenzylideneacetone)dipalladium(0) (0.049 g, 0.054 mmol). The reaction mixture was stirred for 15 min before adding 1,4-dibromobenzene (3.35 g, 14.21 mmol). After stirring for another 15 min, bis(4-*tert*-butylphenyl)amine (1.00 g, 3.55 mmol) was added and the reaction mixture was heated to 90 °C for 15 h. The result was cooled to room

temperature and then poured into a large amount of water for extraction with toluene. The organic layer was collected, washed with water, dried over with MgSO₄ and concentrated to give the crude product. The crude was purified by column chromatography on silica gel with hexane as eluent to afford a white powder **2** with a yield of 46% (0.72 g). ¹H NMR (400 MHz, DMSO-*d*₆) δ 7.37-7.31 (m, 6H), 6.95-6.93 (m, 4H), 6.79 (d, *J* = 9.2 Hz, 2H), 1.25 (s, 18H).

4-(tert-butyl)-N-(4-(tert-butyl)phenyl)-N-(4-(4,4,5,5-tetramethyl-1,3,2-dioxaborolan-2-yl)phenyl)aniline (3). Compound **2** (1.00 g, 2.29 mmol), bis(pinacolato)diboron (0.70 g, 2.76 mmol), potassium acetate (0.67 g, 6.83 mmol), and Pd(dppf)Cl₂ (0.057 g, 0.078 mmol) were dissolved in 1,4-dioxane under nitrogen atmosphere. The reaction mixture was stirred at reflux for 24 h. The result was cooled to room temperature and filtered, followed by extraction with ethyl acetate and water. The combined extracts were dried over with MgSO₄ and concentrated to give the crude product which was further purified by column chromatography on silica gel with EA/hexane (1:20) as eluent to afford a white powder **3** with a yield of 79% (0.88 g). ¹H NMR (400 MHz, DMSO-*d*₆) δ 7.48 (d, *J* = 8.6 Hz, 2H), 7.33 (d, *J* = 8.8 Hz, 4H), 6.96 (d, *J* = 8.8 Hz, 4H), 6.80 (d, *J* = 8.6 Hz, 2H), 1.25-1.24 (m, 30H).

4,4'-(naphtho[1,2-*c*:5,6-*c'*]bis([1,2,5]oxadiazole)-5,10-diyl)bis(*N,N*-bis(4-(tert-butyl)phenyl)aniline) (NOz-t-TPA). A mixture of DiBr-NOz (0.20 g, 0.54 mmol), compound **3** (1.05 g, 2.17 mmol), Pd(PPh₃)₄ (0.044 g, 0.038 mmol), and K₂CO₃ (0.19 g, 1.37 mmol) were dissolved in 1,4-dioxane (24 mL)/ethanol (12 mL)/water (8 mL) under nitrogen atmosphere. The reaction mixture was stirred at reflux overnight and then cooled to room temperature. The solvent was concentrated under reduced pressure to give a crude product. The crude was washed by water and recrystallized from a mixture of dichloromethane/ethanol to get the dark purple powder **NOz-t-TPA** with a

yield of 72% (0.36 g). ^1H NMR (400 MHz, CD_2Cl_2) δ 8.58 (s, 2H), 8.06 (d, $J = 8.8$ Hz, 4H), 7.37 (d, $J = 8.8$ Hz, 8H), 7.16-7.12 (m, 12H), 1.34 (s, 36H). ^{13}C NMR could not be recorded due to the low solubility of **NOz-t-TPA**. HRMS (m/z , FAB, $[\text{M}+\text{H}]^+$) calcd. for $\text{C}_{62}\text{H}_{63}\text{N}_6\text{O}_2$ 923.5013, found 923.4991.

X-ray Crystallography. All crystal X-ray diffraction data were measured on a Bruker Smart CCD diffraction equipped with a graphite monochromator, and the data collection was executed using the SMART program. Cell refinement and data reduction were accomplished by using the SAINT program. The structures were solved by using the SHELXTL/PC package and refined by using full-matrix least squares. The empirical absorption correction was applied with the SADABS routine (part of the SHELXTL program) and the structure was solved by direct methods of using the SHELXTL suite of programs. Hydrogen atoms were placed in calculated positions, and were allowed to ride on the parent atoms. All non-hydrogen atoms were treated anisotropically by full-matrix least-squares on F2.

Photophysical measurement. Steady-state absorption and emission spectra were measured under room temperature with a Hitachi (U-3310) spectrophotometer and an Edinburgh (FS920) fluorimeter, respectively. All wavelength-dependent excitation and emission responses of the fluorimeter have been calibrated. Solvents used for photophysical measurements were spectroscopic grade (Merck Inc.). The quantum yield measurements were conducted with an integrating sphere coupled with Edinburgh (FS920) fluorimeter. The time-resolved measurements were performed by TCSPC system (OB-900L Lifetime spectrometer, Edinburgh). The light source was generated from Ti sapphire laser (Tsunami, Spectra Physics, 82 MHz) pulse-selected to reduce the repetition rate to 0.82 MHz or 82kHz, followed by second harmonic generation to produce excitation beam (357 nm and 380 nm). The polarization of the pump laser was set at the magic angle (54.7°) with respect to pump beam, in order to eliminate the anisotropy. The temporal resolution is about 20 ps.

Computation methodology. All the theoretical calculations were performed using the

Gaussian 09 program. The geometries of the ground states were optimized by the DFT method, and the corresponding absorption wavelength were calculated by the TD-DFT method with CAM-B3LYP hybrid function with polarizable continuum model in cyclohexane. The 6-31+G(d,p) basis set was employed for all atoms.

Cyclic voltammetry measurement. Cyclic voltammograms were obtained using solutions in dry dichloromethane (DCM) or in nitrogen-purged dry N-methyl-2-pyrrolidone (NMP), with tetrabutylammonium perchlorate (TBAP) as the supporting electrolyte (0.1 M). The concentration of analyte was ~ 1 mM for NOz. The working electrode was a glassy carbon electrode. The counter electrode was a Pt wire, and the reference electrode was Ag/AgCl for all analytes.

OLED fabrications. All chemicals were purified through vacuum sublimation prior to use. The OLED were fabricated through vacuum deposition of the materials at 10^{-6} torr onto the ITO-coated glass substrates having a sheet resistance of $15 \Omega \text{ sq}^{-1}$. Prior to use the ITO surface was cleaned ultrasonically; i.e. with acetone, methanol, and deionized water in sequence and finally with UV-ozone. The deposition rate of each organic material was ca. $1 - 2 \text{ \AA} \cdot \text{s}^{-1}$. The $J-V-L$ characteristics of the devices were measured simultaneously in a glove-box using a Keithley 2614B source meter equipped with a calibration Si-photodiode. EL spectra were measured using a photodiode array (Ocean Optics USB2000+).

Simulative Approach.

Deconvolution of data of transient photoluminance. The deconvolution was performed by OriginPro 2016. The raw data of sample ($y(t)$) and IRF ($h(t)$) in time domain measured by TCSPC were first manipulated by Fast Fourier Transformation (FFT) to obtain signal $Y(f)$ and $H(f)$ in frequency domain. The true signal ($X(f)$) in frequency domain could thus be obtained by dividing $Y(f)$ with $H(f)$. By performing inverse Fast Fourier Transformation (IFFT) to $X(f)$, the true signal in time domain $x(t)$, which was the deconvolution of $y(t)$ with IRF ($h(t)$), could be acquired.

Kinetic simulation of Tris-PCz:CN-T2T:dopants (x%) in thin film. The simulation was performed by Wolfram Mathematica 10.1. The experimental data were measured from the time-correlated single photon counting (TCSPC) system (OB-900L Lifetime spectrometer, Edinburgh) with the excitation at 357 nm (repetition rate of 0.82 MHz or 82kHz). Prior to the model fitting, the experimental data were deconvoluted to remove the broadening effect originating from IRF. All fitting values were solved and approximated by interpolating function, which is the default function utilized in solving numerical differentiation equations in the program. The size of each step was adopted, so that the estimated error in the solution was within the tolerance specified by the program. The model fitting of Tris-PCz:CN-T2T can be solved by eqs. (1-2) with the given initial condition $[S^*](t) = 1$, $[T^*](t) = 0$ at $t = 0$. During the fitting process, the parameters were fitted iteratively with one parameter free to fit. The rate constants concerned with thermal activated delayed fluorescence (TADF) process (k_{isc} , k_{risc} , k_f , k_p) could thus be determined (shown in **Figure 5(a)**). For model fitting of Tris-PCz:CN-T2T: 1 wt% dopants (**NOz-t-TPA** or **NOz-TPA**), we assumed the kinetic of energy transfer follow the mechanism depicted in **Figure 5(b)**. Eqs. (4-7) express the rate equations of the proposed model. The equations could be solved by the given initial

condition $[S^*](t) = 1$, $[T^*](t) = 0$, $[DS^*](t) = 0$, $[DT^*](t)$ at $t = 0$. We used the previous fitted TADF kinetic parameters as the initial guess for k_{isc} , k_{risc} , k_f , k_p in the dopant contained model. As we obtained all the rate constants, we fixed all the rate constants and used the initial condition mentioned above to solve eqs. (4-7) and acquired the analytical solutions of photoluminescence. The corresponding results are shown **Figure 5(b)** and eqs. (8-9). The analytical solutions for EL could be obtained by resetting the initial condition to $[S^*](t) = 1$, $[T^*](t) = 3$, $[DS^*](t) = 0$, $[DT^*](t)$ at $t = 0$.

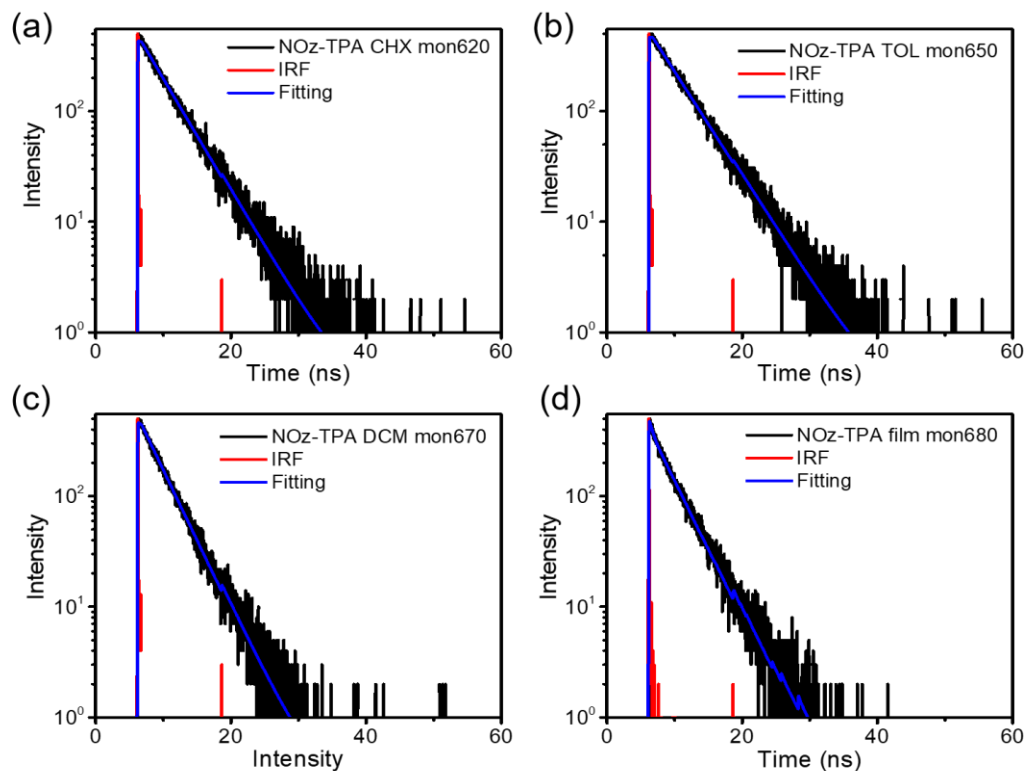


Figure S1. The fluorescence decay dynamics of **NOz-TPA** in (a) CHX, (b) TOL, (c) DCM, and (d) neat thin film at room temperature (RT). CHX, TOL, and DCM denote cyclohexane, toluene, and dichloromethane, respectively. IRF denotes instrument response function. $\lambda_{\text{ex}} = 380$ nm. The fitted lifetimes are tabulated in **Table S1**.

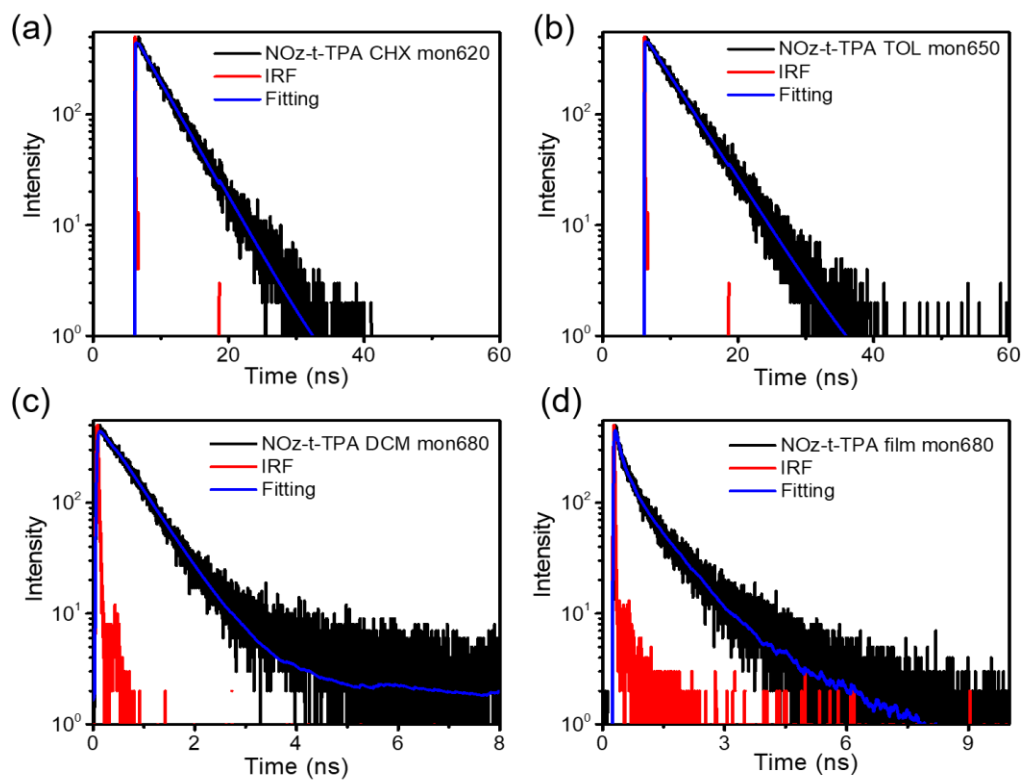


Figure S2. The fluorescence decay dynamics of **NOz-t-TPA** in (a) CHX, (b) TOL, (c) DCM, and (d) neat thin film at RT. $\lambda_{\text{ex}} = 380$ nm. The fitted lifetimes are tabulated in **Table S1**.

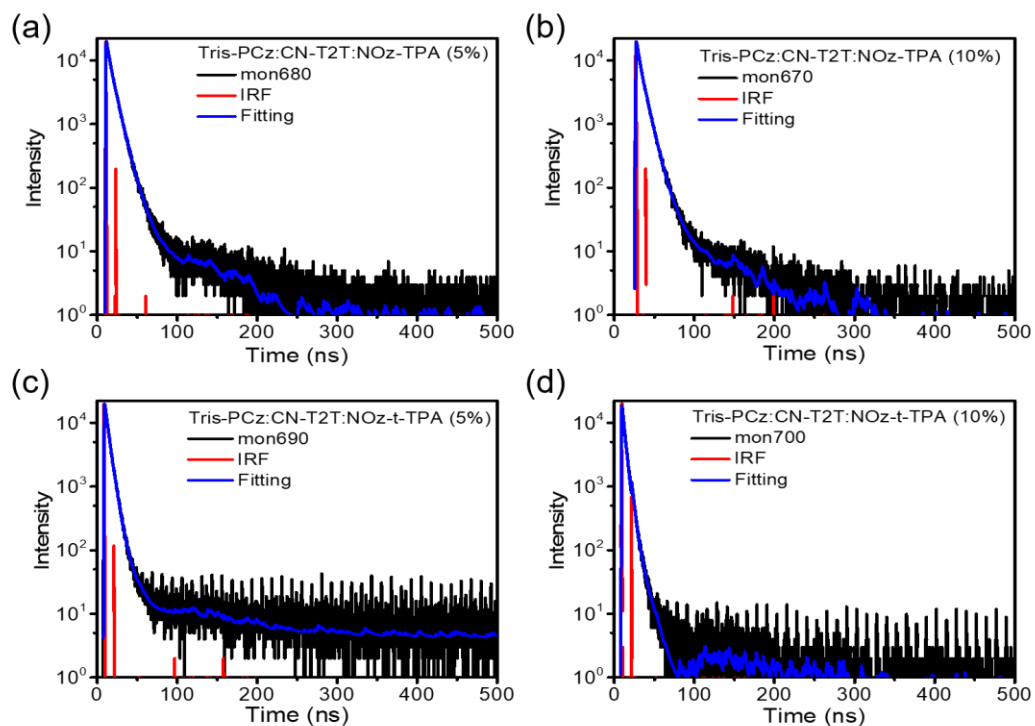


Figure S3. Population lifetime of Tris-PCz:CN-T2T:dopant ((a,b) for **NOz-TPA** and (c,d) for **NOz-t-TPA**) under 5 and 10 wt%. $\lambda_{ex} = 357$ nm.

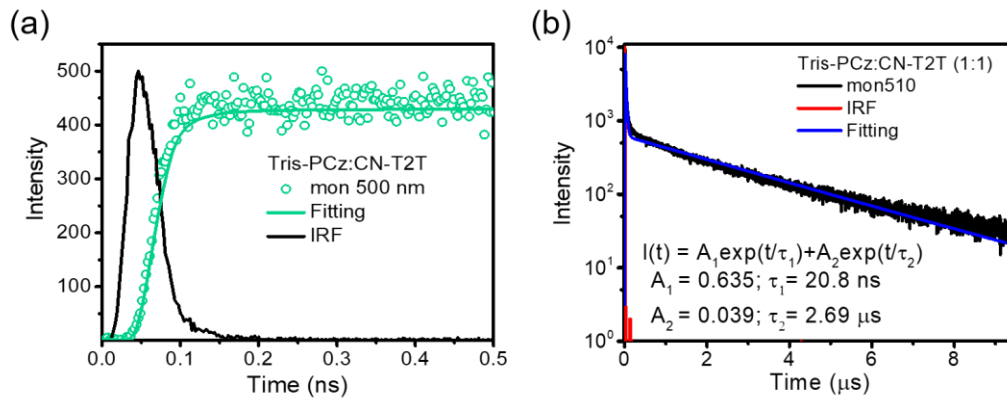


Figure S4. (a) Early dynamic measurement for the formation of charge transfer (CT) state of Tris-PCz:CN-T2T exciplex. The corresponding rise time is irresolvable (< 20 ps). (b) Exponential fit of population lifetime of Tris-PCz:CN-T2T exciplex.

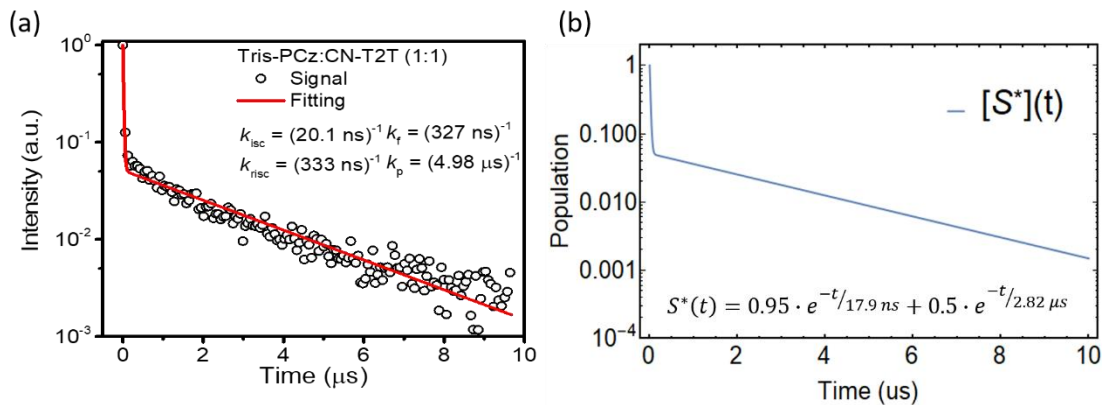


Figure S5. (a) Model fitting of the population decay of S^* of Tris-PCz:CN-T2T. Block circles are the experimental data of Tris-PCz:CN-T2T in thin film monitored at 500 nm. Red line is the model fitting curve based on the proposed model (**Figure 5(a)**). (b) Simulated population decay of Tris-PCz:CN-T2T exciplex with fitted parameters shown in **Figure S5(a)**. The inset is the simulated prompt and delayed lifetime of Tris-PCz:CN-T2T exciplex

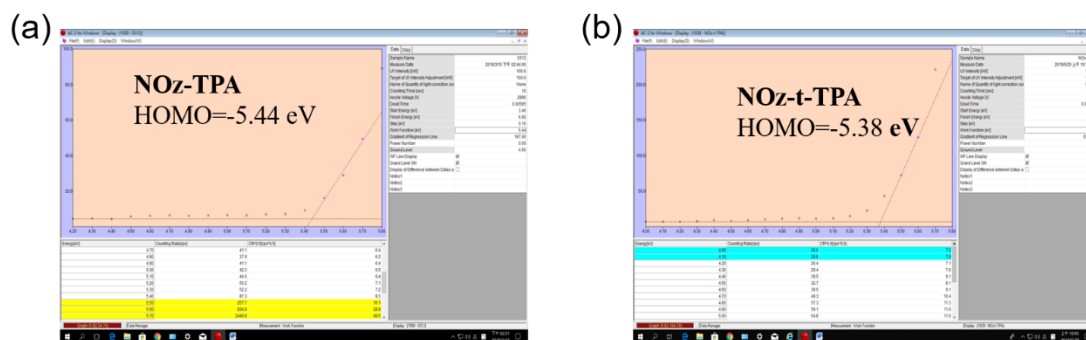


Figure S6. Experimental HOMO value of (a) NOz-TPA and (b) NOz-t-TPA measured by a Riken AC-2 photoelectron spectroscopy (PES).

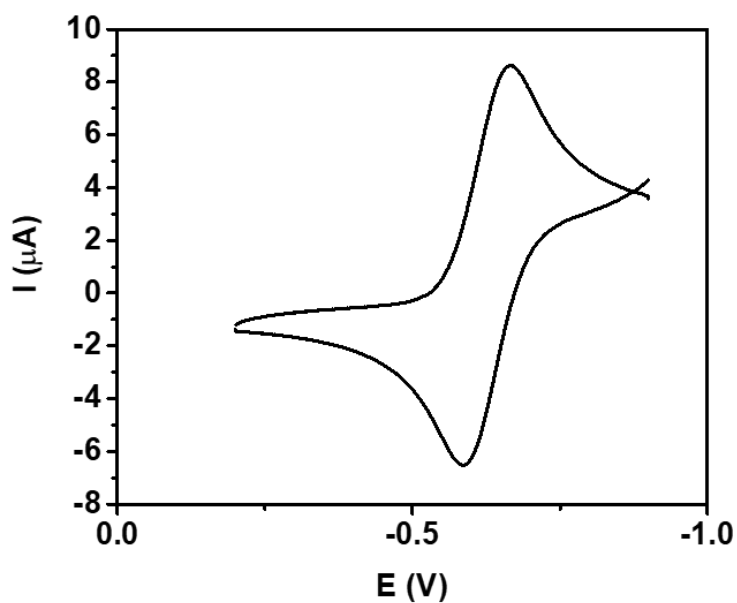


Figure S7. Cyclic voltammograms of NOz. The energy level of LUMO of NOz is calculated to be -3.56 eV. $\text{LUMO} = -e(E_{1/2}^{\text{re}} - E_{1/2, \text{fc}}^{\text{ox}}) + (-4.8) \text{ eV}$, $E_{1/2, \text{fc}}^{\text{ox}} = 0.61 \text{ eV}$ in DCM with 0.1 M TBAP.

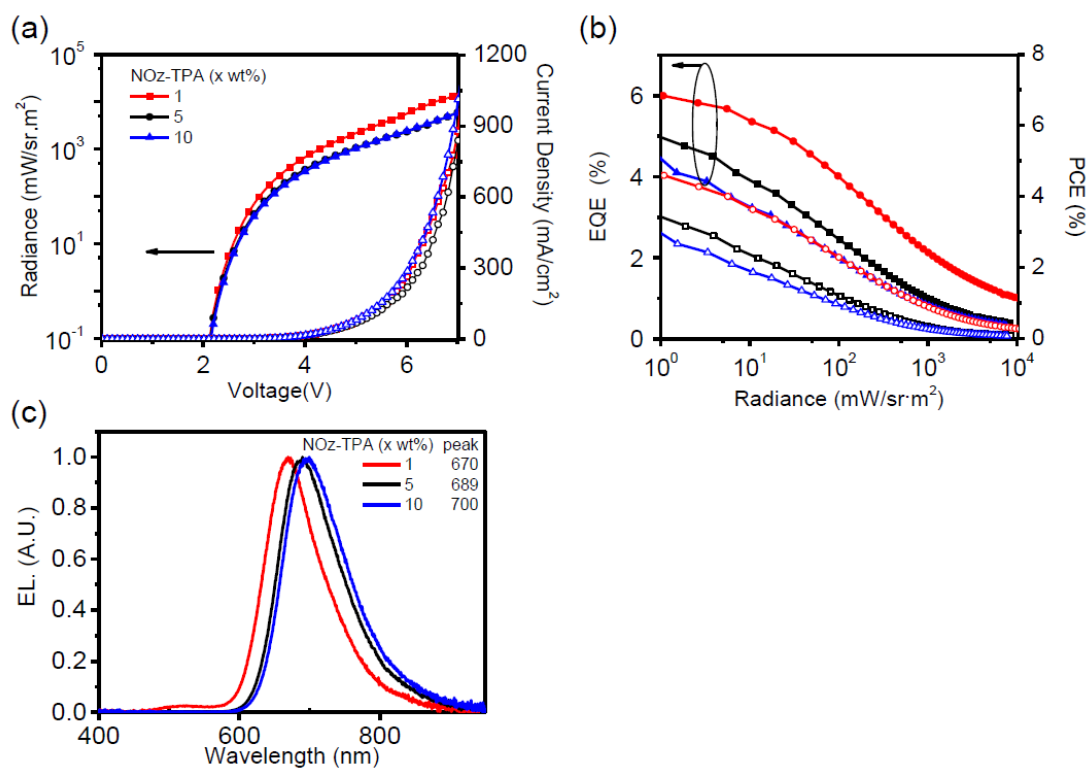


Figure S8. (a) Current density-voltage-radiance (J-V-R) characteristics. (b) External quantum efficiencies (EQE) and power conversion efficiencies (PCE) as a function of luminance, (c) EL spectra of **NOz-TPA** devices.

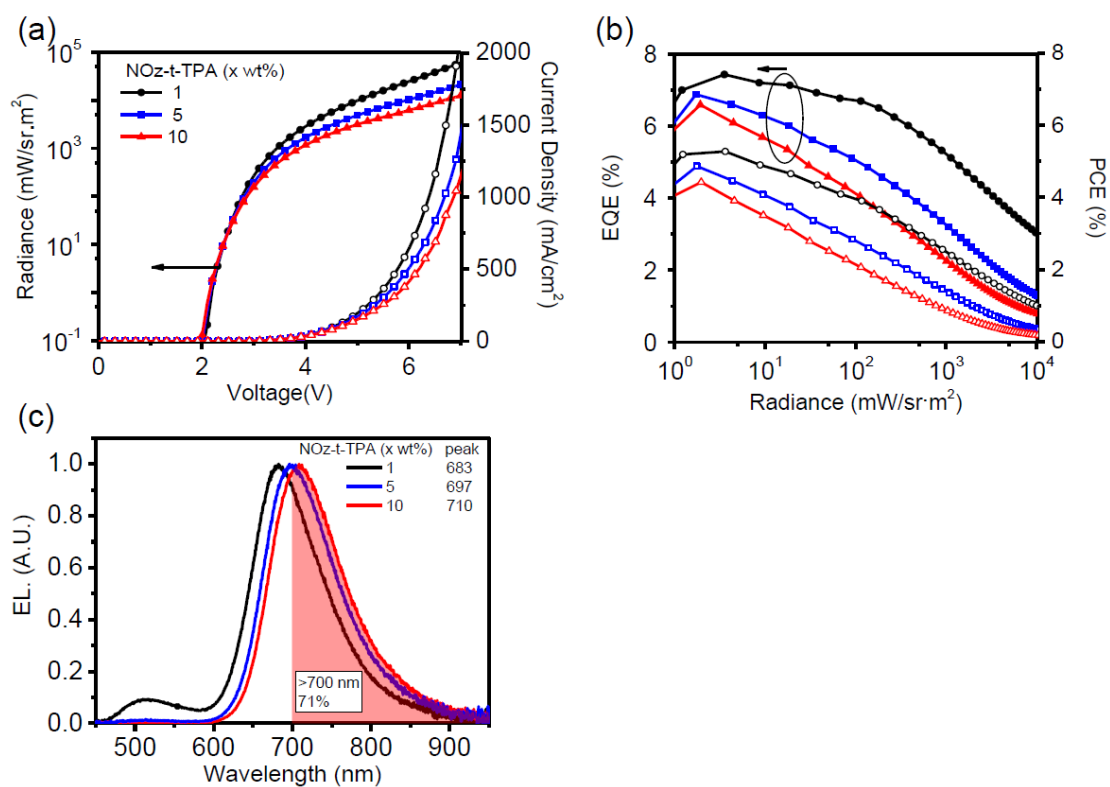


Figure S9. (a) Current density-voltage-radiance (J-V-R) characteristics. (b) External quantum efficiencies (EQE) and power conversion efficiencies (PCE) as a function of luminance, (c) EL spectra of **NOz-t-TPA** devices.

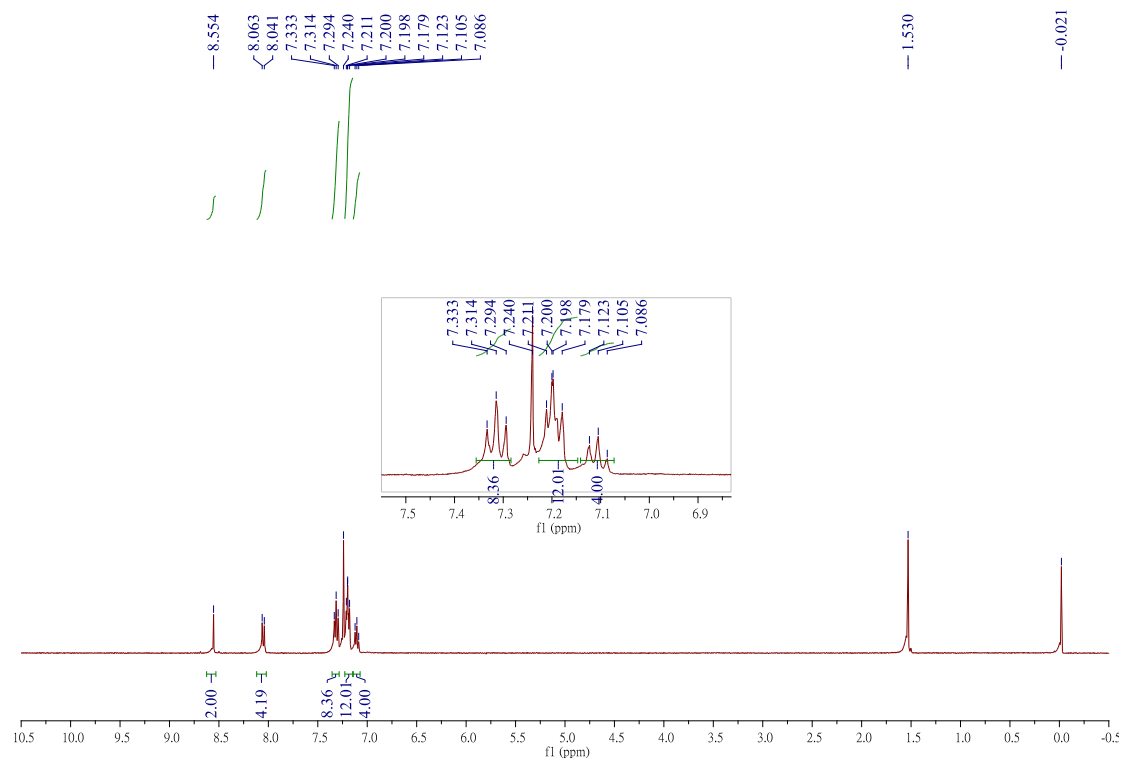


Figure S10. $^1\text{H-NMR}$ spectrum of **NOz-TPA** in CDCl_3

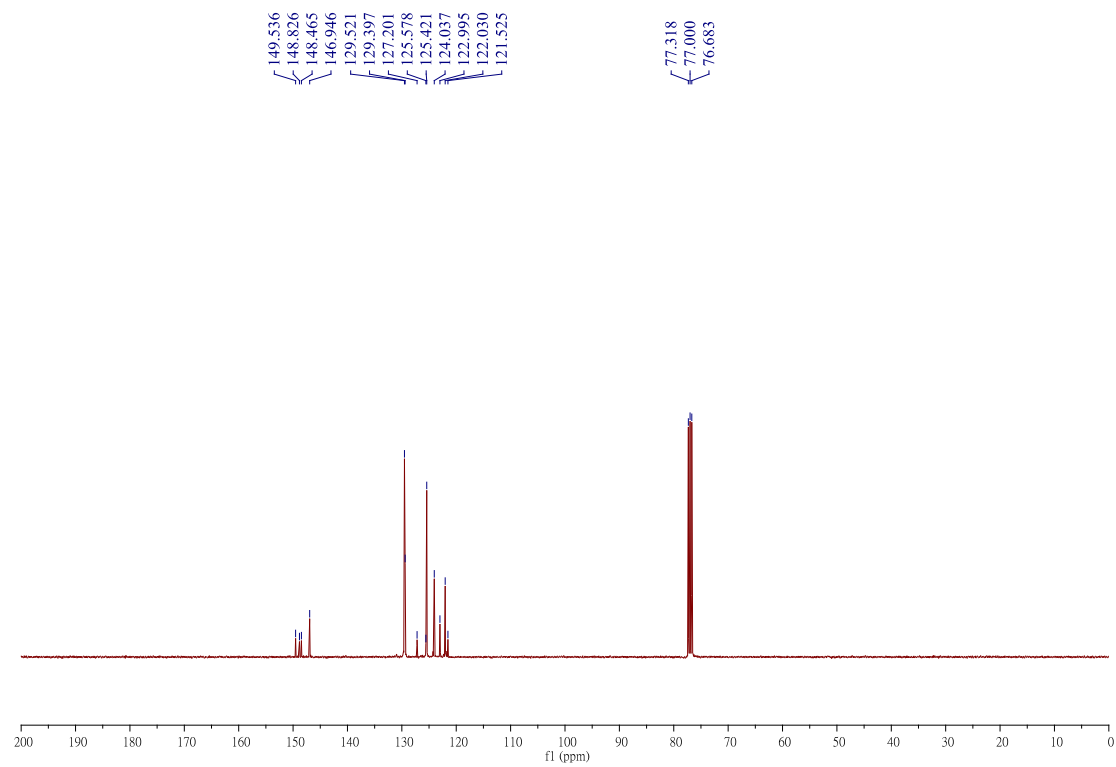


Figure S11. $^{13}\text{C-NMR}$ spectrum of **NOz-TPA** in CDCl_3

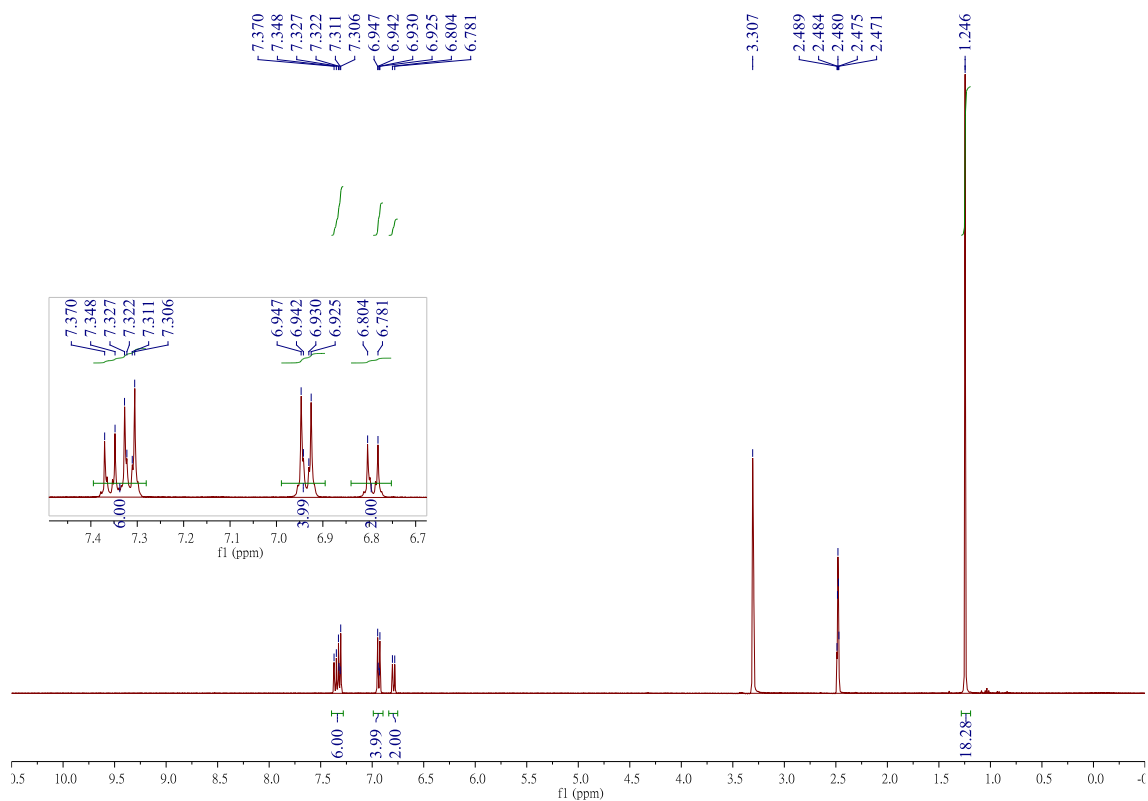


Figure S12. $^1\text{H-NMR}$ spectrum of compound **2** in $\text{DMSO-}d_6$.

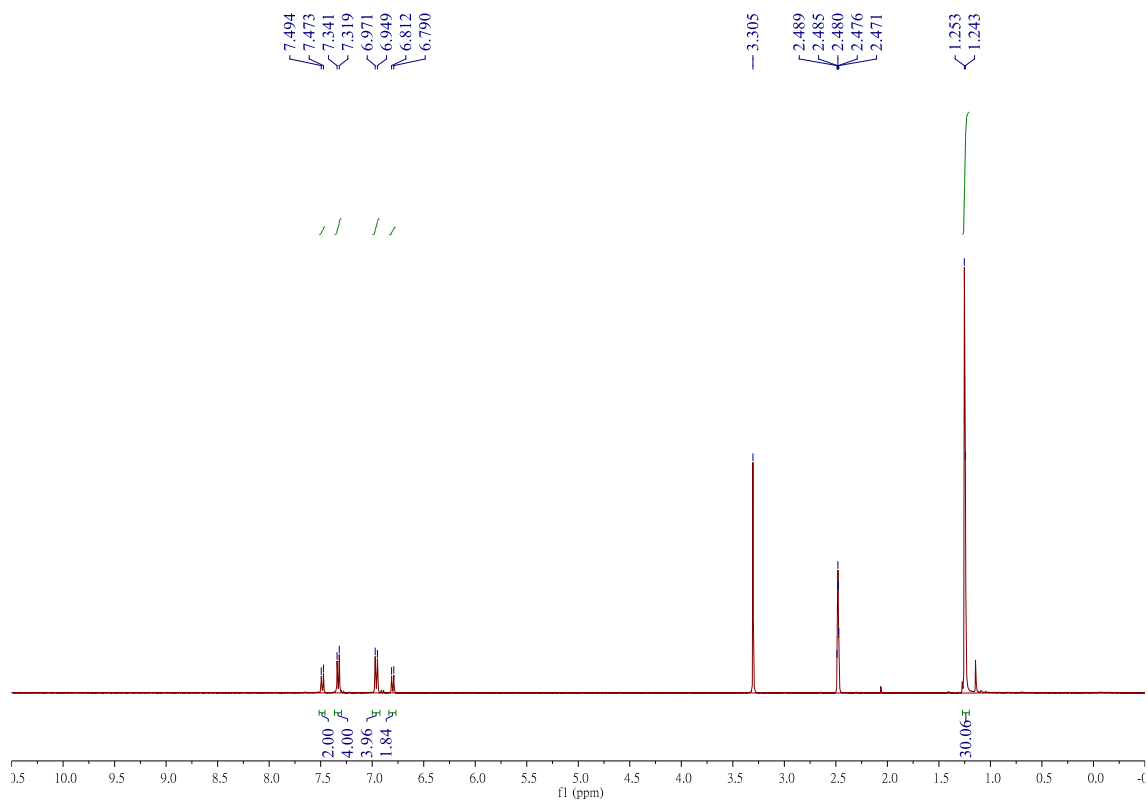


Figure S13. $^1\text{H-NMR}$ spectrum of compound **3** in $\text{DMSO-}d_6$.

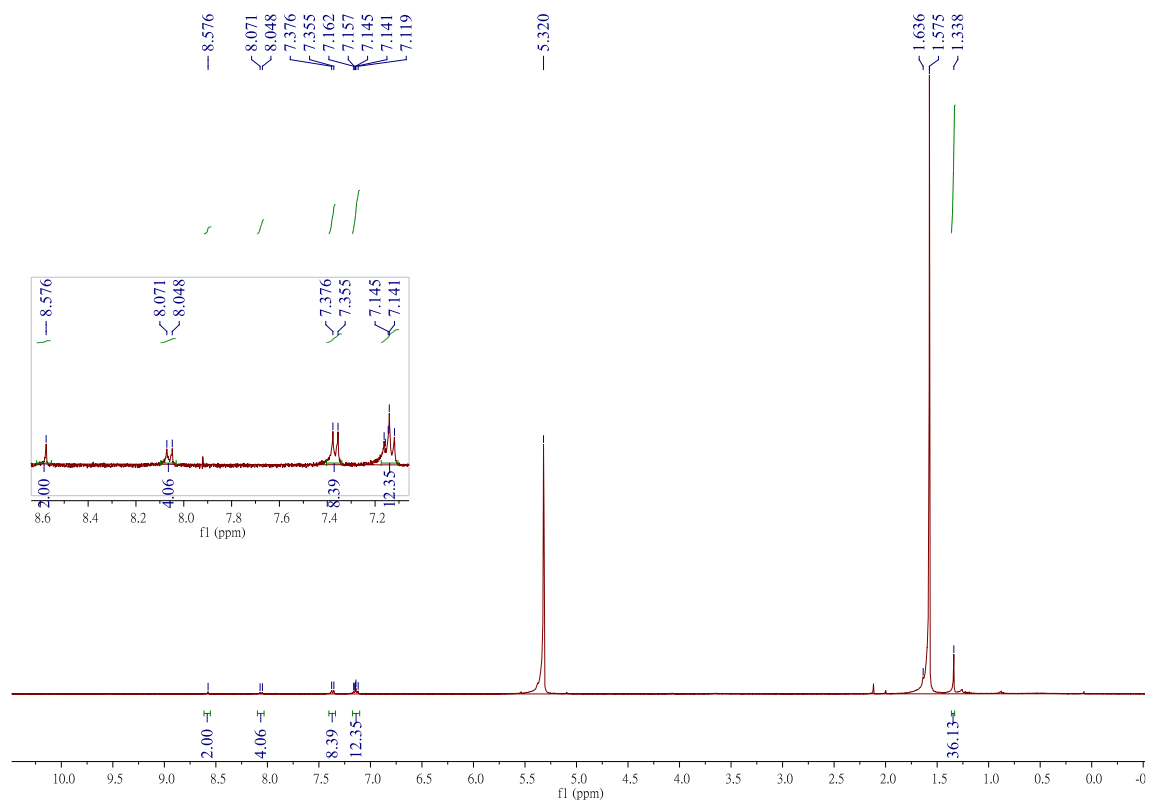


Figure S14. $^1\text{H-NMR}$ spectrum of NOz-t-TPA in CD_2Cl_2 .

Table S1. Selected photophysical properties of **NOz-TPA** and **NOz-t-TPA** measured at RT.

compound	Abs (nm) ^a	Em (nm) ^b	Φ (%) ^c	τ (ns)	ϵ (cm ⁻¹ M ⁻¹) ^d	
NOz-TPA	CHX	542	603	66	4.18	
	TOL	548	653	40	4.54	
	DCM	548	746	5.5	3.29	22100
	Film	570	730	22	0.43 (30%) 3.44 (70%)	
NOz-t-TPA	CHX	564	622	56	4.05	
	TOL	570	675	35	4.59	
	DCM	573	800	0.9	0.61	20900
	Film	586	750	6.8	0.16 (71%) 0.82 (29%)	

^aThe absorption wavelength measured at the peak of the first absorption band.

^bThe emission wavelength measured at the peak.

^cQuantum yield of the corresponding emission band.

^dThe extinction coefficients were measured in DCM due to the poor solubility in cyclohexane and toluene.

Table S2. Optimized structure of **NOz-TPA** and **NOz-t-TPA** in ground states (S_0) and the corresponding frontier orbitals.

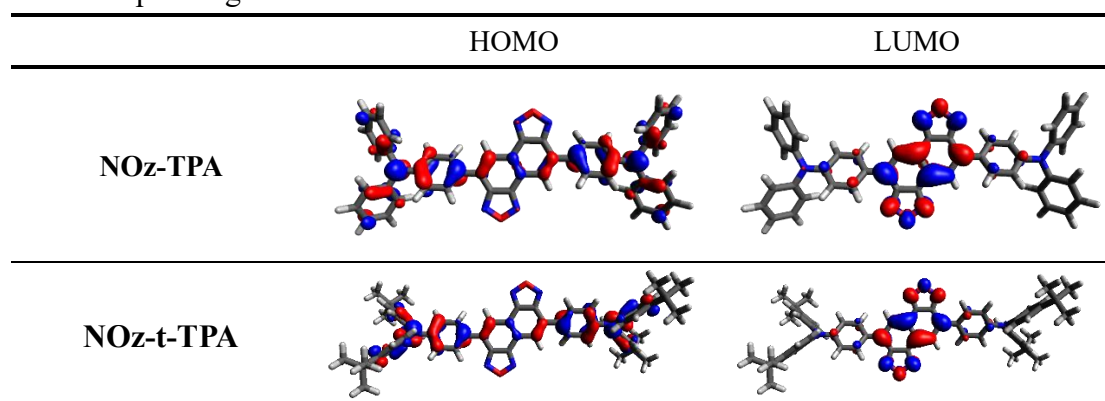


Table S3. Model Fitting Parameters.

	k_{isc}	k_{rise}	k_f	k_p	k_{FE}	k_{DE}	k_{df}	k_{dp}
Host	(20.1 ns) ⁻¹	(333 ns) ⁻¹	(327 ns) ⁻¹	(4.98 μs) ⁻¹	~	~	~	~
NOz-TPA	(11.0 ns) ⁻¹	(217 ns) ⁻¹	(323 ns) ⁻¹	(7.14 μs) ⁻¹	(0.77 ns) ⁻¹	(0.44 μs) ⁻¹	(10.8 ns) ⁻¹	(10 μs) ⁻¹
NOz-t-TPA	(11.0 ns) ⁻¹	(217 ns) ⁻¹	(323 ns) ⁻¹	(7.14 μs) ⁻¹	(1.05 ns) ⁻¹	(26.0 μs) ⁻¹	(9.71 ns) ⁻¹	(10 μs) ⁻¹

Table S4. The experimental orbital energy levels for **NOz-TPA** and **NOz-t-TPA**.^a

compound	HOMO ^b	LUMO ^c
NOz-TPA	-5.44	-3.64
NOz-t-TPA	-5.38	-3.61

^aNotes that the energy levels were recorded as unit of e.V.

^bThe HOMO energy was obtained from photoelectron spectroscopy (PES) measurements.

^cThe LUMO energy was obtained by adding the absorption gap measured from the solid thin film to the corresponding HOMO energy.